NeuroImage 295 (2024) 120662

Contents lists available at ScienceDirect

NeuroImage

journal homepage: www.elsevier.com/locate/ynimg

Mouse brain elastography changes with sleep/wake cycles, aging, and Alzheimer's disease

Gary R. Ge [a], Wei Song [b], Michael J. Giannetto [b], Jannick P. Rolland [a,c,d], Maiken Nedergaard [b,e,*], Kevin J. Parker [c,f,g,**]

[a] The Institute of Optics, University of Rochester, 480 Intercampus Drive, Rochester, NY 14627, USA
[b] Center for Translational Neuromedicine, University of Rochester Medical Center, 601 Elmwood Avenue, Rochester, NY 14642, USA
[c] Department of Biomedical Engineering, University of Rochester, 204 Robert B. Goergen Hall, Rochester, NY 14627, USA
[d] Center for Visual Science, University of Rochester, 361 Meliora Hall, Rochester, NY 14627, USA
[e] Center for Translational Neuromedicine, University of Copenhagen, Blegdamsvej 3B, 2200-N, Denmark
[f] Department of Electrical and Computer Engineering, University of Rochester, 500 Computer Studies Building, Rochester, NY 14627, USA
[g] Department of Imaging Sciences (Radiology), University of Rochester Medical Center, 601 Elmwood Avenue, Rochester, NY 14642, USA

ARTICLE INFO

Keywords:
Brain elastography
Aging
Sleep/wake cycle
Alzheimer's disease

ABSTRACT

Understanding the physiological processes in aging and how neurodegenerative disorders affect cognitive function is a high priority for advancing human health. One specific area of recently enabled research is the *in vivo* biomechanical state of the brain. This study utilized reverberant optical coherence elastography, a high-resolution elasticity imaging method, to investigate stiffness changes during the sleep/wake cycle, aging, and Alzheimer's disease in murine models. Four-dimensional scans of 44 wildtype mice, 13 mice with deletion of aquaporin-4 water channel, and 12 mice with Alzheimer-related pathology (APP/PS1) demonstrated that (1) cortical tissue became *softer* (on the order of a 10% decrease in shear wave speed) when young wildtype mice transitioned from wake to anesthetized, yet this effect was lost in aging and with mice overexpressing amyloid-β or lacking the water channel AQP4. (2) Cortical stiffness *increased* with age in all mice lines, but wildtype mice exhibited the most prominent changes as a function of aging. The study provides novel insight into the brain's biomechanics, the constraints of fluid flow, and how the state of brain activity affects basic properties of cortical tissues.

1. Introduction

Dementia is a complex and heterogeneous group of brain disorders broadly characterized by a decline in cognitive functions. Symptoms include memory loss, cognitive impairment, and behavioral or personality changes that interfere with activities of daily living (van der Flier et al., 2023). Abnormal changes in the brain can occur decades before the clinical syndrome becomes apparent (Beason-Held et al., 2013). One hypothesis regarding the cause of dementia is glymphatic failure (Nedergaard and Goldman 2020). The glymphatic system is a recently discovered pathway that enables cerebrospinal fluid (CSF) flow in the brain and this fluid transport is thought to be key in regulating waste clearance, e.g., of amyloid-β found in Alzheimer's disease (AD) and other physiological brain pathways (Xie et al., 2013; Mestre et al., 2020; Hablitz and Nedergaard 2021; Rasmussen et al., 2021). CSF flow is supported by aquaporin-4 (AQP4) water channels that are localized at the perivascular astrocytic endfeet (Mestre et al., 2018). The glymphatic system is active during sleep, suppressed during wakefulness (Xie et al., 2013), and regulated by circadian rhythm via increased vascular AQP4 polarization (Hablitz et al., 2020). Furthermore, waste clearance and glymphatic influx were found to be reduced, indicating glymphatic impairment in both aging and AD-related pathologies (Kress et al., 2014; Ma et al., 2017; Reeves et al., 2020). Recent glymphatic studies have focused on fluid transport and dynamics in the brain (Bohr et al., 2022; Kedarasetti et al., 2022; Bojarskaite et al., 2023) to better understand the physiology of its regulation and constraints (Thomas 2022; Tithof et al., 2022). One potential area to address is how the biomechanical properties of the brain may influence glymphatic flow and vice-versa. To gain a

* Corresponding author at: Center for Translational Neuromedicine, University of Rochester Medical Center, 601 Elmwood Avenue, Rochester, NY 14642, USA.
** Corresponding author at: Department of Biomedical Engineering, University of Rochester, 204 Robert B. Goergen Hall, Rochester, NY 14627, USA.
E-mail addresses: nedergaard@URMC.Rochester.edu (M. Nedergaard), kevin.parker@rochester.edu (K.J. Parker).

https://doi.org/10.1016/j.neuroimage.2024.120662
Received 27 February 2024; Received in revised form 5 May 2024; Accepted 30 May 2024
Available online 31 May 2024

better understanding of the physical mechanisms underlying how the glymphatic system contributes to aging and AD, elastography was used here to analyze the biomechanical properties of the brain.

Elastography is the technique of imaging mechanical wave disturbances (such as shear waves) introduced into the tissue. Elasticity, the main biomechanical property of interest, represents the softness or stiffness of a material, and can be estimated directly from the shear wave speed (SWS) (Ormachea and Parker 2020). Elastic changes are known to occur in certain diseases (e.g., liver cirrhosis and tumor environments), and elastography has been useful in providing diagnostic information (Doyley and Parker 2014). Recent literature reviews reveal that *in vivo* studies of the brain's mechanical properties have primarily been completed with magnetic resonance elastography (MRE) with few studies using ultrasound (Clayton et al., 2011; Clayton et al., 2012; Hiscox et al., 2016; Low et al., 2016; Bigot et al., 2018; Ertl et al., 2018; Tzschätzsch et al., 2018; Murphy et al., 2019; Hiscox et al., 2021; Sack 2023). The general consensus (albeit not unanimous) is that the adult human brain softens with age, particularly in later decades of life (Sack et al., 2011; Arani et al., 2015; Hiscox et al., 2018; Guo et al., 2019; Takamura et al., 2019). Decreases in stiffness with AD are also observed (Murphy et al., 2011; Murphy et al., 2012; ElSheikh et al., 2017; Gerischer et al., 2018; Coelho and Sousa 2022) in both rodent models and humans. Some recent studies indicate that maturation in mice is associated with increased stiffness using MRE and atomic force microscopy (Guo et al., 2019; Segel et al., 2019). Thus, additional studies using alternative methodologies are needed to further explore these trends.

Another modality that may prove useful for brain elastography specifically in mice studies is optical coherence elastography (OCE). OCE is based on the optical coherence tomography (OCT) system, which uses broadband lasers to image biological tissues based on the scattering properties of light (Huang et al. 1991). Volumetric data can be obtained with lateral and axial resolutions of a few microns (Fujimoto et al., 2000; Zysk et al., 2007; Murali et al., 2009; Rolland et al., 2010; Xu et al., 2021). The significant increase in lateral and axial resolutions compared to MRE comes at a cost of reduced depth penetration to a few millimeters and typically a reduced field of view (FOV). An additional cost for brain studies specifically is the invasive nature secondary to requiring a cranial window. While the FOV and depth penetration could be limitations in OCE, significant information regarding changes in cortical brain tissue can be ascertained in mice due to their thin cortex. OCE is a recent development that has already been demonstrated for many biological and clinical applications; studies have been performed in cornea, skin, heart, muscle, and breast (Kennedy et al., 2009; Ford et al., 2011; Kennedy et al., 2011; Kennedy et al., 2013; Wang and Larin 2015; Zvietcovich and Larin 2022; Leartprapun and Adie 2023). A significant example of this is the elasticity mapping of individual corneal layers (Zvietcovich et al. 2019). Recent studies have shown that OCE can be applied to brain studies as well (Zvietcovich et al. 2019; Ge et al., 2022; Ge et al., 2023).

In a recently published study, a theoretical basis for linking brain elastography to fluid dynamics was established (Ge et al., 2022). Our hypothesis is that the stiffness of the brain, as measured by shear wave elastography, is a sensitive measure of the regulation or dysregulation of fluid dispersion, particularly within the glymphatic system. Specifically, we expect that changes in brain stiffness are correlated with CSF influx changes in the sleep/wake cycle, physiological aging, and disease pathologies. In this study, we utilize OCE to determine how the wake versus anesthesia states, aging, AQP4 deficiency, and AD-related pathology influence cortical brain tissue stiffness in wildtype and non-wildtype mice strains and compared the observations to previous reports on glymphatic flow. A specific elastography approach using reverberant shear waves is utilized – reverberant OCE has demonstrated high resolution capabilities by measuring the elasticity of individual layers of cornea as well as identifying perivascular versus parenchymal regions of the brain (Zvietcovich et al. 2019; Ge et al., 2022; Ge et al., 2023). Reverberant OCE takes advantage of the boundary reflections of shear waves often observed in tissue elastograms, which is useful for analyzing heterogeneous and complex soft tissues such as the brain (Parker et al., 2017; Ormachea et al., 2018). We report here that tissue stiffness changes are strongly correlated with aging, AQP4 deficiency, AD pathology, and perhaps most interestingly with the state of brain activity.

2. Materials and methods

2.1. Animal preparation

A total of 35 wildtype mice (C57BL/6, ranging from 2.5 to 30.6 months of age, 22 male/13 female), 12 AQP4 homozygous knockout (KO) mice ($Aqp4^{-/-}$, ranging from 3.0 to 22.0 months of age, 7 male/5 female), 7 AQP4 heterozygous (Het) mice ($Aqp4^{+/-}$, ranging from 4.0 to 8.0 months of age, 4 male/3 female), and 12 mice with Alzheimer-related pathology (APP/PS1, ranging from 7.0 to 30.9 months of age, 5 male/7 female) were scanned during both awake and anesthetized (mimicking sleep (Xie et al., 2013), or NREM sleep-like) states. In addition, 9 wildtype mice (C57BL6, ranging from 3.0 to 22.4 months of age, 5 male/4 female) and 1 AQP4 homozygous KO mouse ($Aqp4^{-/-}$, 5.8 months of age, male) were scanned during the awake state only. This information is also tabulated in Supplemental Table S1. The AQP4-KO, AQP4-Het, and APP/PS1 mice were confirmed with tail genotyping. The C57BL/6 mice were purchased (Charles River Laboratories, Wilmington, Massachusetts, USA), as well as the APP/PS1 mice (Jackson Laboratory, Bar Harbor, Maine, USA). Both strains were bred in-house. The AQP4 mice are maintained at the University of Rochester vivarium on a C57BL/6 background and described by Thrane et al. (2011).

Mice were trained to the scanning and elastography apparatus prior to surgery. Experiments were performed within a 4 h time frame, starting around 10:00 and ending before 14:00. Cranial window surgeries were performed in which glass cover slips ranging from 5 to 8 mm in diameter replaced a parietal skull portion leaning on top of the right hemisphere near the center superior sagittal sinus (centered on AP = -2.5, ML = 2.5 mm relative to bregma), while leaving the dura mater intact. A 1.1% agarose gel solution in sterile saline was used to adhere the glass window to the brain and skull. A rectangular head plate and mounting station was used to secure the mouse head during both awake and anesthetized states. A custom holder was used to contain the mouse body, allowing for comfortable measures while restricting movement. Optical scans were performed 30 min post-surgery for the awake state, and 15 min post-anesthesia (ketamine-xylazine or KX cocktail, 100 mg/kg ketamine, 20 mg/kg xylazine, administered intraperitoneally) for the anesthetized state. Upon anesthetized state scan completion, the mice were euthanized, and the brains were extracted to measure brain water content. The wet and dry weights in grams (w_{wet} and w_{dry}) were measured at the time of euthanasia and after 72 h incubation at 65 °C in a preheated oven, respectively. Brain water content was computed as $\frac{w_{wet}-w_{dry}}{w_{wet}} \times 100\%$. Mice experiments were performed under protocols approved by the University of Rochester Committee on Animal Resources (under protocol number 101914 / 2011-023E). Similar details regarding related animal preparation are previously described by Ge *et al*, which also used a small portion of the dataset presented in this study (Ge et al., 2022).

2.2. Optical coherence tomography

A custom phase-sensitive OCT system is used to obtain volumetric B-mode scans. The OCT system is implemented with a swept-source laser (HSL-2100-HW, Santec, Aichi, Japan) that has a center wavelength of 1310 nm and a bandwidth of 140 nm. The lateral resolution is estimated to be approximately 20 μm and the axial resolution is measured to be approximately 6 μm in air. It has an imaging depth of up to 2 mm in the brain. The A-line (i.e., axial depth) acquisition rate is 50 kHz and the

mean output power is 15 mW. The square FOV for these experiments ranged from approximately 3 × 3 to 6 × 6 mm, optimized based on the cranial window placement and visualization of the real-time B-mode images. The OCT system is controlled using LabVIEW (version 14, National Instruments, Austin, Texas, USA). A schematic of the OCT system is shown in Supplemental Fig. S1.

2.3. Reverberant shear wave elastography

In conjunction with the OCT system described above, a mechanical piezo-electric system is used to perform reverberant shear wave elastography. A custom 3D printed ring with 8 concentric points of contact is used as the mechanical source to generate multiple shear waves. It is 10 mm in diameter in size, with an 8 mm internal aperture to allow for OCT laser scanning. Each of the rings' tips are in physical contact with the agarose gel/glue that is in contact with the glass window/skull/brain interfaces, but is not in contact with the glass window, skull, nor brain. A function generator (AFG320, Tektronix, Beaverton, Oregon, USA) along with a power amplifier (PDu150, PiezoDrive, Callaghan, New South Wales, Australia) was used to submit waves of 2 kHz frequency. Supplemental Fig. S2 demonstrates this configuration. The MB mode approach allows for acquisition of 4D data (i.e., 3D space and time) in a synchronized fashion, generating 100 A-lines × 100 frames × 2000 points in axial depth × 100 M-modes. The total OCE scan time is approximately 8 min, with an additional 10–15 min to transfer the data from memory to disk (where the computer cannot undergo another scan simultaneously). This 4D data can then be used to obtain 4D particle velocity data via an algorithm by Loupas et al. (1995), which is then subsequently used to obtain elastography data.

2.4. Data processing

For each 3D spatial frame in an individual point of time in which a fully developed reverberant pattern is present, 2D local spatial autocorrelations in the *x-y* plane are performed with varying window sizes, ranging from 0.1 × 0.1 mm to 4 × 4 mm, with varying intervals ranging from 0.2 × 0.2 mm to 0.5 × 0.5 mm, along each point in depth. The exact window size and interval combination was selected based on the FOV and contours of the B-mode intensities. From this information, a 3D map of local wavenumbers was extracted, which was then converted to a local SWS value. Select frames in time were then averaged to obtain a finalized 3D elastogram. Supplemental Fig. S3 shows the basic processing pipeline. More details on this methodology are adapted from previous studies (Zvietcovich et al. 2019; Ge et al., 2022). Elastogram estimations and data processing are completed in MATLAB 2022b (Mathworks, Natick, MA, USA). Elastography and data processing code are available from the authors upon completion of a data sharing agreement.

2.5. Data and statistical analysis

For each 3D elastogram, a mean SWS is reported using rectangular volume masks that visually contain mostly homogeneous brain parenchyma. Entire cohorts of data (with each mouse representing a point) are summarized by plotting parameters (age, measured SWS in awake or anesthetized states, and brain water content). Linear fitting along with coefficient of determination R^2 scores are reported for correlating trends in wildtype mice. Pearson correlation coefficient r and associated p-value for each linear correlation are reported as well. Fisher transformation is performed to compare Pearson correlations, and one-tailed p-values are reported. Confidence intervals (CI) of 95% are reported for slopes of linear fits. Relevant statistical tests used for comparison of groups (e.g., between sex, strains) include the Kruskal-Wallis test with post-hoc Bonferroni-corrected Dunn's test. Statistical significances are assigned as follows: no significance (NS) for $p > 0.5$, * for $p < 0.05$, ** for $p < 0.01$, *** for $p < 0.001$, and **** for $p < 0.0001$. Data and statistical analysis are performed using Python 3.11.1 (Python Software Foundation, Wilmington, Delaware, USA). Resulting data is provided in an Excel sheet as part of the Supplementary Materials.

3. Results

3.1. Sample images and elastograms

Sample 3D B-mode scans, reverberant shear wave fields, and elastograms obtained from a female 8-month-old APP/PS1 mouse are shown in Supplemental Figs. S4 (awake state) and S5 (anesthetized state). Two-dimensional average intensity projections (AIP) of the 3D B-modes and elastograms are shown in Fig. 1. The AIPs are convenient for visualizing the vasculature seen in the cortical surface along with stiffer regions of brain parenchyma. While arterial walls in isolation are expected to be stiffer than the interstitium, the contents of the vessels (blood, CSF) and the inherent spatial averaging contribute to the SWS measured as shown in Fig. 1. Another example of a male 9-month-old C57BL/6 mouse is shown in Supplemental Fig. S6, in which the elastograms are more homogeneous than those in Fig. 1.

3.2. Awake vs. KX anesthesia patterns

For each mouse, the reported mean SWS is used as the representative measurement. Higher SWS values are indicative of increased stiffness. During the initial stages of data collection, statistical tests were performed to see if there were biological sex differences. There were no statistical differences in stiffness measurements or computed brain water content of all mouse strains between male and female biological sex. This is consistent with a prior study in which biological sex was not found to impact glymphatic function in aging (Giannetto et al., 2020). However, it is known that APP/PS1 mice do show a sex difference in which female mice accumulate amyloid-β at an earlier age and accumulate more deposits in the hippocampus (Wang et al., 2003). This sex difference was not observed in the APP/PS1 experiments of this study, likely due to the fact that only cortical brain was able to be scanned due to the 2 mm depth penetration of the OCE system and local plaque severity determines glymphatic impairment (Peng et al., 2016; Mestre et al., 2022).

Fig. 2 summarizes all mouse data with both awake and anesthetized SWS measurements. Anesthetized SWS is plotted versus awake SWS for ease of visualizing SWS change between the two states. The size of data points is proportional to the age of the mouse. Overall, there is a strong positive correlation ($r = 0.95,\ p < 0.0001$) between measured SWS values in the two states for the wildtype C57BL/6 strain, as well as for each of the other strains (see Supplemental Table S2 for complete statistics). Stiffness during anesthesia is highly correlated with stiffness while awake. A modified version of Fig. 2 is shown in Supplemental Fig. S7, where linear fits for all strains are shown.

Visually, the C57BL/6 linear fit is lower than the black line of unity slope, indicating that measured SWS in anesthesia is decreased from that of the awake state (the cortical brains become softer during anesthesia). This trend is seen at least partially for all strains. However, the linear slopes of the C57BL/6 (1.04, CI [0.92, 1.16]) and AQP4-Het (1.07, CI [0.74, 1.40] strains are closer to 1.0 than the AQP4-KO (1.43, CI [0.96, 1.90]) and APP/PS1 (1.51, CI [0.93, 2.09]) strains (however, all include unity in the confidence intervals), all with high R^2 values (Supplemental Table S2 and Supplemental Fig. S7). In the relevant range of values represented, the linear curve fits for C57BL/6 and AQP4-Het strains do not cross the black unity line, while the AQP4-KO and APP/PS1 do. This indicates that while C57BL/6 and AQP4-Het strains show softer brains during anesthesia for most mice, at some point in either age or stiffness, this ceases to be true for AQP4-KO and APP/PS1 mice, of which some see no change in SWS between anesthesia and awake. This can be confirmed visually from Fig. 2.

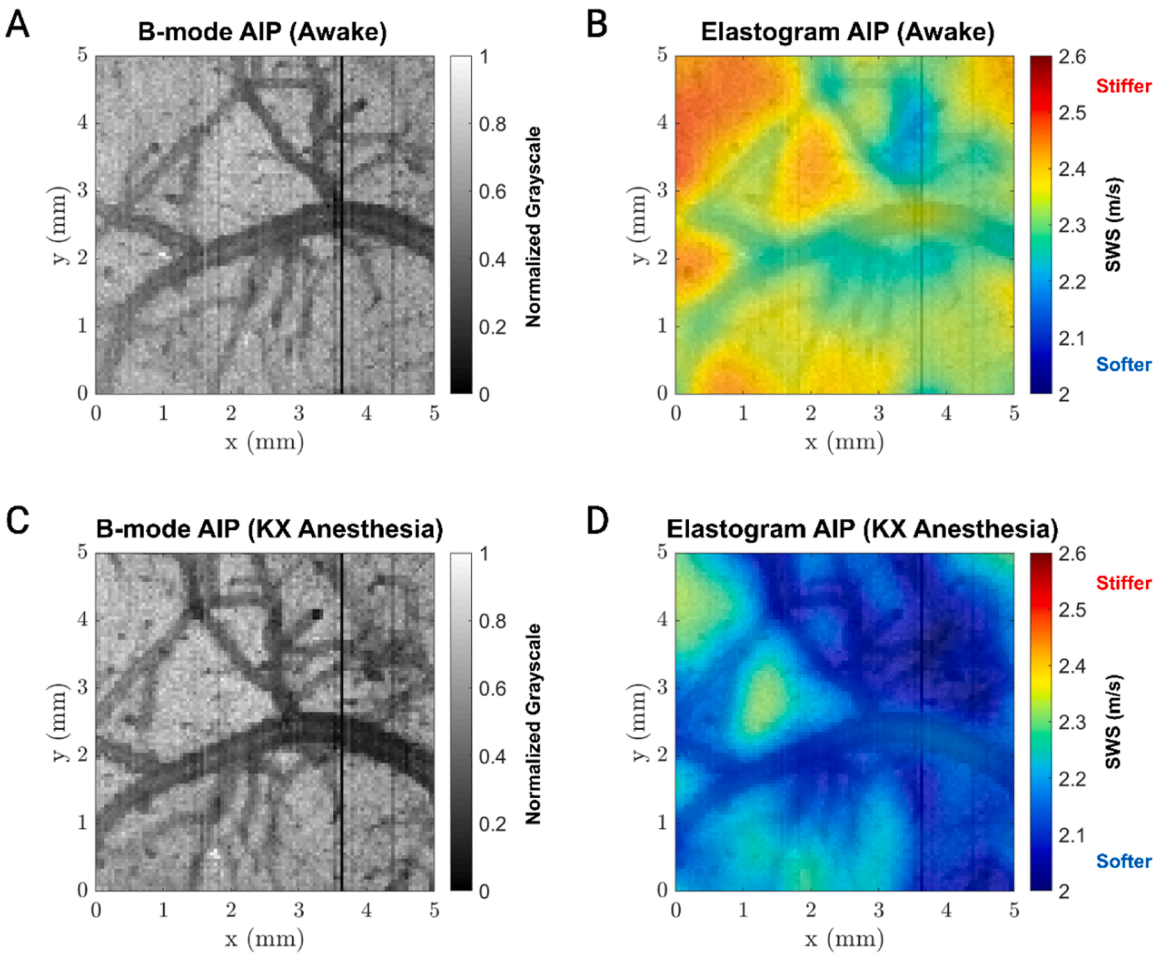

Fig. 1. Sample images from a female, 8 months of age, APP/PS1 mouse. (A) Average intensity projection (AIP) of 3D B-mode scan during awake state. (B) AIP of 3D elastogram during awake state. The mean SWS is 2.30 ± 0.05 m/s from the entire volume. (C) AIP of 3D B-mode scan during KX anesthesia. (D) AIP of the 3D elastogram during KX anesthesia. The mean SWS is 2.12 ± 0.08 m/s from the entire volume. Volumetric scans of upper 200 μm of cortical brain from which these AIPs are derived are shown in Supplemental Figs. S4 and S5.

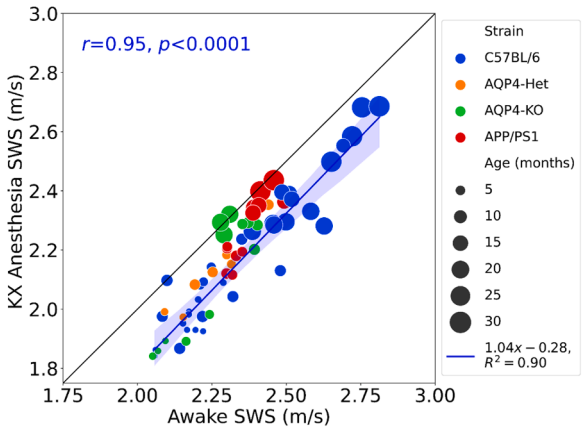

Fig. 2. Summary data for measured SWS in awake and anesthesia states. The black line with unity slope indicates a state of no SWS change between awake and anesthesia states. The 4 strains are represented by colors (blue for wildtype C57BL6, orange for AQP4-Het, green for AQP4-KO, and red for APP/PS1). The size of the data points is proportional to the age, with larger points denoting older age. The blue line is a linear curve fit with a blue shade representing the 99% confidence interval for the fit. The equation for the line is $1.04x - 0.28$ with an R^2 value of 0.90. The Pearson correlation coefficient is $r = 0.95$ with $p < 0.0001$ for the wildtype strain.

Finally, it is apparent that in general, stiffness increases with age for all strains. It is noted that the stiffness between strains seems to be different. Notably, older wildtype C57BL/6 mice tend to have stiffer brains than the older AQP4-KO and APP/PS1 mice. These relationships are further explored in the following sections.

3.3. Brain water content and measured SWS as a function of age

Fig. 3 shows plots of brain water content, anesthetized SWS, and awake SWS as a function of mouse age. A modified version of Fig. 3 is shown in Supplemental Fig. S8, in which linear fits for all strains are shown. In Fig. 3A, there is a strong negative correlation between brain water content and age for C57BL/6 mice ($r = -0.87, p < 0.0001$). This correlation is preserved for all strains except the APP/PS1 mice (NS) and is noted to be weaker for AQP4-KO mice with $r = -0.61$ (vs. C57BL/6 mice with $p = 0.0455$). The C57BL/6 and AQP4-Het have modest R^2 values for their respective linear curve fits, while the AQP4-KO and APP/PS1 mice have poor fits (Supplemental Table S2 and Supplemental Fig. S8). The linear slopes are steeper for C57BL/6 (-0.084, CI : $[-0.099, -0.069]$) than the APP/PS1 (-0.010, CI : $[-0.037, 0.016]$) strains. In other words, the C57BL/6 strain has a more pronounced decrease in brain water content as they age than the APP/PS1 strain.

In Fig. 3B, there is a strong positive correlation between anesthetized SWS and age for C57BL/6 mice ($r = 0.89, p < 0.0001$). This correlation is present for all strains (NS for pairwise comparisons among correlation coefficients of different strains). The C57BL/6 and APP/PS1 strains

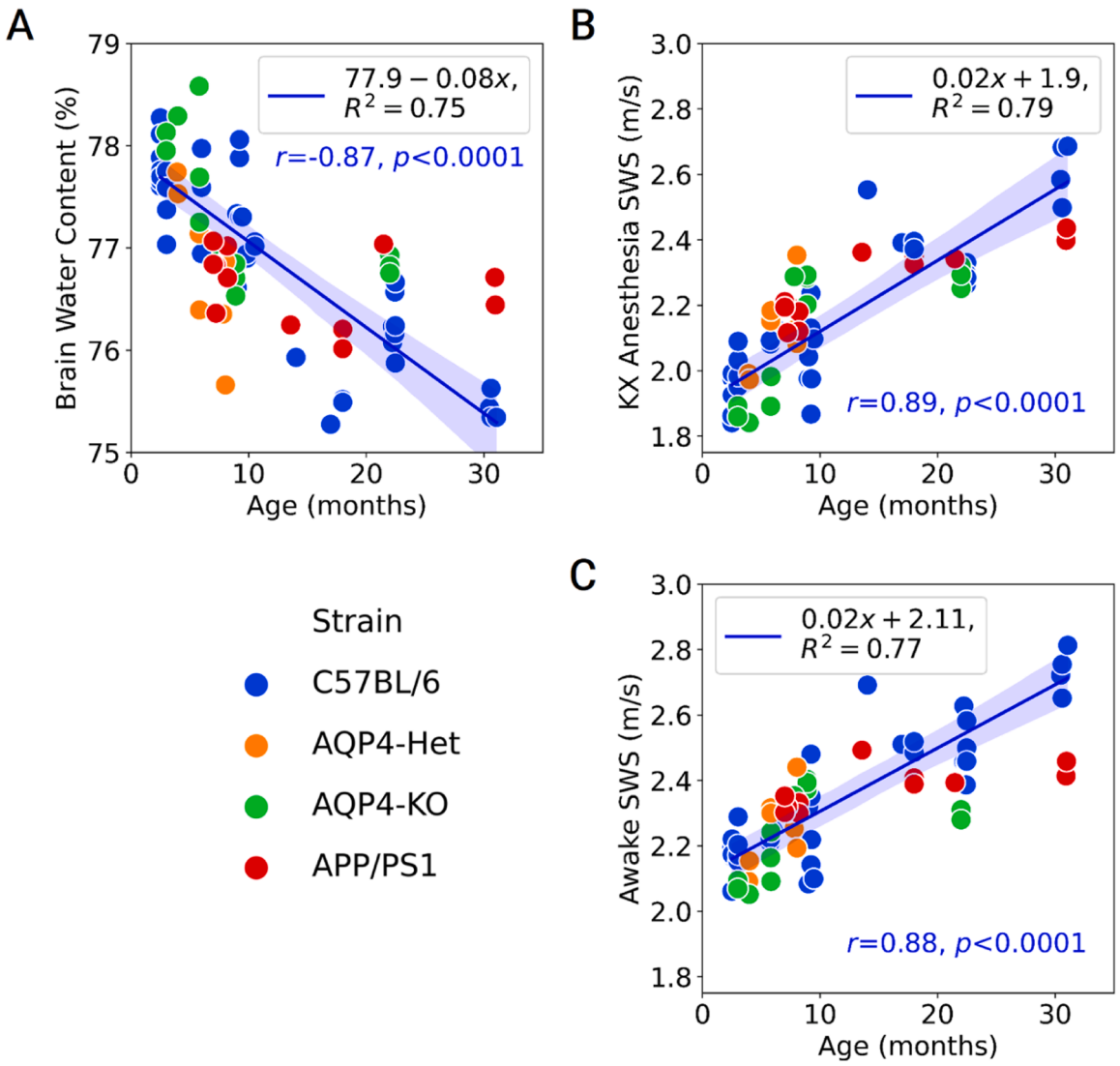

Fig. 3. Summary data for measured SWS and brain water content as functions of age. The 4 strains are represented by colors (blue for wildtype C57BL6, orange for AQP4-Het, green for AQP4-KO, and red for APP/PS1). The blue line is a linear curve fit with a blue shade representing the 99% confidence interval for the fit. (A) Brain water content as a function of age. The equation for the line is $77.87 - 0.08x$ with an R^2 value of 0.75. The Pearson correlation coefficient is $r = -0.87$ with $p < 0.0001$. (B) KX anesthesia SWS as a function of age. The equation for the line is $0.02x + 1.90$ with an R^2 value of 0.79. The Pearson correlation coefficient is $r = 0.89$ with $p < 0.0001$. (C) Awake SWS as a function of age. The equation for the line is $0.02x + 2.11$ with an R^2 value of 0.77. The Pearson correlation coefficient is $r = 0.88$ with $p < 0.0001$. These measurements are reported for the wildtype C57BL/6 strain.

exhibit moderate R^2 values for their respective linear curve fits, and the slope of the C57BL/6 $(0.022,\ CI : [0.018,\ 0.026])$ is steeper than that of the APP/PS1 $(0.011,\ CI : [0.007,\ 0.015])$ (Supplemental Table S2 and Supplemental Fig. S8). Thus, C57BL/6 mice brains grow stiffer as a function of age compared with the APP/PS1 brains.

Fig. 3C shows very similar results as Fig. 3B. There is a strong positive correlation between awake SWS and age for C57BL/6 mice ($r = 0.88, p < 0.0001$). There is a weaker positive correlation for the APP/PS1 mice when compared with C57BL/6 ($p = 0.011$), and other strains have statistically insignificant correlations. Only the C57BL/6 strain has a moderate R^2 value for its linear curve fit, the rest have low values (Supplemental Table S2 and Supplemental Fig. S8). Linear slopes from both Fig. 3B and C, from highest to lowest, are ordered as follows: AQP4-Het, C57BL/6, AQP4-KO, and APP/PS1. This suggests that certain strains (AQP4-KO, APP/PS1) do not grow as stiff over a mouse lifetime as others (C57BL6, AQP4-Het).

3.4. Measured SWS post-anesthesia as a function of brain water content

Both measured SWS in anesthesia and change in SWS are plotted as a function of global brain water content that was measured after the anesthesia state and euthanasia in Fig. 4. A modified version of Fig. 4 is shown in Supplemental Fig. S9, in which linear fits for all strains are shown. As expected, there is a strong negative correlation between anesthetized SWS and brain water content in C57BL/6 mice ($r = -0.93,\ p < 0.0001$), shown in Fig. 4A. This correlation holds for the AQP4-Het and AQP4-KO strains but becomes statistically insignificant for the APP/PS1 strain (Supplemental Table S2). In addition, all strains except the APP/PS1 mice have high R^2 values for their respective linear curve fits. The slopes of C57BL/6 $(-0.237,\ CI : [-0.270,\ -0.205])$, AQP4-KO $(-0.0266,\ CI : [-0.321,\ -0.211])$, and AQP4-Het $(-0.161,\ CI : [-0.243,\ -0.078])$ strains demonstrate similar negative slopes, whereas a negative slope for the APP/PS1 strain $(-0.122,\ CI : [-0.321,\ 0.077])$ is not completely statistically supported.

In Fig. 4B, the change in SWS, defined as $\frac{(SWS_{anesthetized} - SWS_{awake})}{SWS_{awake}} \times 100\%$,

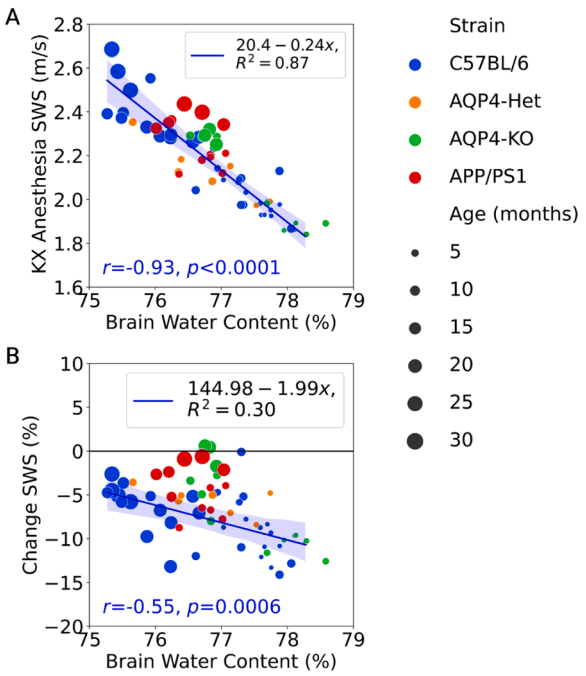

Fig. 4. Summary data for SWS and brain water content. The 4 strains are represented by colors (blue for wildtype C57BL6, orange for AQP4-Het, green for AQP4-KO, and red for APP/PS1). The size of the data points is proportional to the age, with larger points denoting older age. The blue line is a linear curve fit with a blue shade representing the 99% confidence interval for the fit. (A) KX anesthesia SWS is plotted as a function of brain water content. The equation for the blue line is $20.4 - 0.24x$ with an R^2 value of 0.87. The Pearson correlation coefficient is $r = -0.93$ with $p < 0.0001$. (B) Change in SWS, defined as $\frac{(SWS_{anesthetized} - SWS_{awake})}{SWS_{awake}} \times 100\%$ is plotted as a function of brain water content. The black line represents no change in SWS. The equation for the blue line is $144.98 - 1.99x$ with an R^2 value of 0.30. The Pearson correlation coefficient is $r = -0.55$ with $p < 0.001$. These measurements are reported for the wildtype C57BL/6 strain.

is plotted as a function of brain water content. Most data points fall below the black line representing the zero line, indicating that most have a negative change in SWS, i.e., cortical brain gets softer during anesthesia. Many older AQP4-KO and APP/PS1 mice trend closer towards the zero line, as well as a lone C57BL/6 mouse. However, the correlation between change in SWS and brain water is much weaker (insignificant for AQP4-Het and APP/PS1 mice), and all strains have low R^2 values for their respective linear curve fits (Supplemental Table S2 and Supplemental Fig. S9). This is due to the involvement of the awake SWS value, which at baseline, is not expected to be correlated with brain water content, since the brain was not in the awake state at the time of brain extraction for measuring brain water content.

3.5. Summary table of all trends

Table 1 provides a summary of general trends. The left column represents trends found in this study. The right column describes additional studies or comments that complement the findings in the left column. In addition, further statistical testing of wildtype (C57BL/6) and non-wildtype (AQP4-KO and APP/PS1) groups per age category are performed and shown in Supplemental Fig. S10. While statistical power is lost from grouping into generalized age categories (0–9 months for young, 9–18 months for middle-aged, and 18+ months for old), statistically significant differences between wildtype and non-wildtype old mice as well as between young and old mice are still present in brain water content and SWS measurements.

Table 1
Summary of trends.

Experimental Findings	Corroborating Reports and Effects
Cortical brain gets *softer* from awake to anesthesia (sleep-like) in all strains of young mice. This effect is preserved into old ages in C57BL/6 and AQP4-Het strains (Figs. 2, 4B).	- Glymphatic influx increases during sleep or ketamine/xylazine anesthesia in C57BL/6 mice (Hablitz et al., 2019). - AQP4-Het mice have not been extensively studied but thought to be physiologically similar to wildtype.
In AQP4-KO and APP/PS1 strains, cortical brain gets *softer* from awake to sleep-like anesthesia in younger mice (<10 months), but this effect is lost for some older mice (> 10 months) (Figs. 2, 4B).	- Recent studies indicate there is decreased CSF influx in AQP4-KO (Mestre et al., 2018; Silva et al. 2021). - Glymphatic fluid transport is suppressed in APP/PS1 mice (Peng et al., 2016). Waste such as amyloid-β accumulate rapidly in these mice as they age (Xu et al., 2015). - Age-specific (i.e., which month of age) reduction in glymphatic influx in non-wildtype mice strains have been documented between 3 and 20 months, but not specifically established (Benveniste et al., 2019; Giannetto et al., 2020, Rasmussen et al., 2021).
Stiffness increases with age in all strains. There is a smaller increase in AQP4-KO and APP/PS1 mice than when compared with C57BL/6 mice (Figs. 2, 3B and 3C).	- Some previous MRE studies find that stiffness decreases with old age in human brains (Hiscox et al., 2018; Takamura et al., 2019). - Some studies in mice indicate increased stiffness with age (Guo et al., 2019; Segel et al., 2019). - MRE studies in humans are generally supportive of the notion that certain regional stiffness (e.g., in the hippocampus) decreases more significantly in AD and other neurodegenerative diseases with age (Gerischer et al., 2018; Murphy et al., 2019).
Global brain water content decreases with age in all strains except APP/PS1 mice. C57BL/6 has a higher decrease in brain water content over time than the AQP4-KO and APP/PS1 strains (Fig. 3A).	- Brain water content decreases with age in normal rats (Gottschalk et al., 2021). - Glymphatic influx decreases with age (Kress et al., 2014; Giannetto et al., 2020). - As mentioned previously, glymphatic influx decreases significantly in AQP4-KO and APP/PS1 mice when compared with wildtype mice (Peng et al., 2016; Mestre et al., 2018; Silva et al., 2021).
Stiffness during anesthesia is negatively correlated with global brain water content measured after anesthesia in all strains except APP/PS1 mice. (Fig. 4A)	- It is accepted from physical principles that increased water content as a percentage will lead to softer tissues. However, the exact physical equation to describe this relationship has yet to be determined. Efforts are ongoing to analyze the general relationship between water, vascular volume, protein, gliosis, and fat content with viscoelasticity.
Stiffness change between awake and anesthetized states is not well correlated with global brain water content measured after anesthesia in all strains (Fig. 4B).	- It is hypothesized that brain stiffness will vary with activity level and the environment in the awake state. However, there are minimal studies to confirm this and establish a general pattern or trend.
Stiffness measured during anesthesia is highly correlated with stiffness measured while awake for all strains (Fig. 2).	- This suggests that inter-strain and intra-strain variations are not present in relative SWS measurements.
No sex differences found in cortical brain stiffness measurements or global brain water content in C57BL/6, AQP4-HET, AQP4-KO, and APP/PS1 groups.	- No sex differences in glymphatic influx in C57BL/6 mice as a function of age (Giannetto et al., 2020). - No sex differences are mentioned in AQP4 studies (Thrane et al., 2011; Mestre et al., 2018). - Female APP/PS1 mice accumulate more amyloid-β in the hippocampus than males

(*continued on next page*)

Table 1 (*continued*)

Experimental Findings	Corroborating Reports and Effects
	and start at an earlier age (Wang et al., 2003). However, sex studies involving the glymphatic system in APP/PS1 have not been adequately reported.

4. Discussion and conclusions

This study identified key correlations present in subtle stiffness changes seen in sleep-like anesthesia/wake states, aging, and disease from a mouse model using reverberant OCE. These key generalized observations include: (1) cortical brain becomes softer from wake to sleep-like states in wildtype mice; this effect is lost for older mice with either AQP4 deficiency or AD-related pathology, (2) cortical brain stiffness increases with age in all mice, but less changes are observed in mice with AQP4 deficiency and AD-related pathology, (3) global brain water content decreases as a function of age in wildtype mice, but less so in mice with AQP4 deficiency or AD-related pathology, (4) stiffness is strongly negatively linearly correlated with global brain water content in anesthesia; yet this correlation is lost in mice with AD-related pathology, (5) mice have variable cortical brain stiffness during the awake state that is not well correlated with brain water content, and (6) no sex differences are seen in cortical brain stiffness measurements in all strains of mice. The majority of these observations are consistent either with previous studies or with reasonable physical intuition (Table 1) and our quantitative rheological model that accounts for fluid channels (Ge et al., 2022; Ge et al., 2023). To summarize our main hypothesis for the underlying mechanisms associated with our findings and prior work, Fig. 5 illustrates the glymphatic fluid network in normal, aging, and in abnormal conditions along with generalized correlates regarding stiffness:

We now compare our results with previous elastographic studies. First, our results are based on OCT scans, employing the highest spatial resolution and SNR among the common elastography imaging systems (Wang and Larin 2015). Also, the increasing stiffness of the cortical gray matter in mouse that we measured is consistent with the well-known trend of cardiovascular stiffness vs. age in humans (Mitchell et al., 2004) and mice (Santelices et al., 2008). However, our data seemingly contradict some previous studies in humans and rodents (Murphy et al., 2012) whereby brain stiffness *decreases* in the elderly, contrary to the aging trend in our wildtype and non-wildtype mouse models. This raises questions with regard to the differences between mouse and human aging, and whether these differences are physiological and/or pathological in nature (e.g., do apparently healthy humans in later decades of life exhibit some extent of biological disease, inflammation, and dysregulation of the glymphatic system, whereas mice at 30 months do not

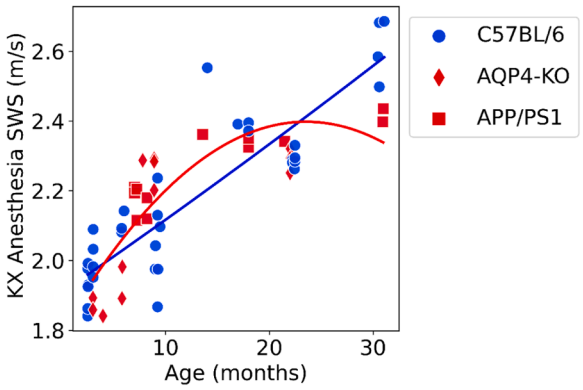

Fig. 6. Summary of stiffness data points of wildtype C57BL/6 mice (as blue circles) and non-wildtype AQP4-KO and APP/PS1 mice (as red diamonds and squares, respectively) as a function of age. Second-order polynomials are fitted to each group. The equation of best fit for the wildtype group in blue is $0.00004x^2 + 0.0205x + 1.91$, with an R^2 value of 0.79. Note that this equation is essentially linear. The equation of best fit for the non-wildtype group in red is $-0.0011x^2 + 0.0505x + 1.8$, with an R^2 value of 0.71. This equation is nonlinear and has a characteristic inverted "U" shape.

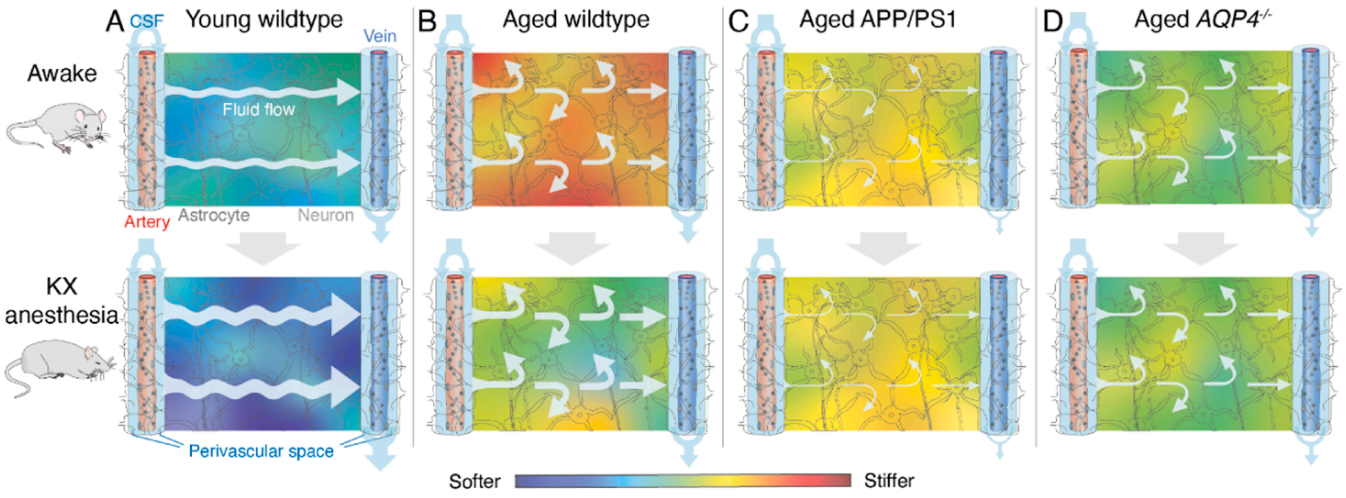

Fig. 5. Observations of glymphatic flow and elasticity in young wildtype, aged wildtype, aged APP/PS1, and aged AQP4 KO mice. (A) In young and healthy mice, cerebrospinal fluid (CSF) enters the brain parenchyma via periarterial pathways, washes out solutes from the interstitial space, and empties along the veins (Rasmussen et al., 2021). Fluid flow and volume are increased during sleep-like states (Xie et al., 2013), effectively reducing hydrodynamic resistance and shear wave speed (Ge, Song et al. 2022). (B) With aging, glymphatic function is reduced (Kress et al., 2014), in part due to astrocytes becoming reactive and AQP4 de-polarization. This, along with decreasing water weight fraction, results in increased tissue stiffness, but with a preserved elastic change between brain states (i.e., softer tissue during sleep or sleep-like states). (C) In AD-related pathology, amyloid-β accumulates in the perivascular spaces (vascular amyloidosis) and in the parenchyma suppressing glymphatic flow (Jessen et al., 2015). The combination of these effects along with protein and waste accumulation, and slightly higher water weight fraction, result in overall softer tissues when compared with aged awake wildtype counterparts. Furthermore, there is a loss of glymphatic activity (Peng et al., 2016, Nedergaard and Goldman 2020) and lack of elastic change during sleep or sleep-like anesthetized states. (D) AQP4 knockout mice demonstrates similar trends with APP/PS1 mice. No stiffness changes are observed between wake and sleep-like brain states, consistent with the impairment of glymphatic activation (Xu et al., 2015; Mestre et al., 2018; Silva et al. 2021).

exhibit these conditions to the same extent?). In Fig. 6, a summary plot of measured stiffness between wildtype and non-wildtype groups is shown. While the red curve represents a group of non-wildtype mice with either AQP4 deficiency or AD-related pathology, it is possible that this curve also resembles "normal" human aging, with sharper stiffness declines expected in abnormal human brains. One might speculate that there is a typical amount of cell death with "normal" aging in humans, and wildtype mice would exhibit this effect simply if they lived longer, while non-wildtype mice just have an acceleration of this effect. The second reason is that the MRE studies, due to their larger FOV and full brain depth penetration, have interrogated many more regional areas of the brain. The focus of this study was on the cortical brain, and it is quite possible that dissimilar trends would be found in other regions. Along a similar vein, brain OCE in this study examines cortex that is inaccessible by MRE, and ultimately demonstrated interesting effects in areas of the brain that have not been fully investigated by MRE.

Limitations of the study reported here include (1) the use of short-term cranial windows combined with effects of surgery and the elastography apparatus, (2) the limited depth penetration of OCE, and (3) lack of simultaneous *in vivo* quantification of other brain parameters. While we have attempted to minimize the pain and duration associated with the experiments, the mouse brain's physiological state in both awake and anesthetized states can be affected by these procedures. The depth penetration of the OCE system limits scans to the upper 2 mm of brain tissue. However, 2 mm captures most, if not all, of the mouse cortex (5-6 layers) (Lerch et al., 2008). While the dura mater was removed, it is also possible some of the OCE measurements include residual meningeal and extra-neuronal structures. Finally, this study does not involve other parameters that might be relevant, such as quantification of amyloid-β plaques using immunohistochemistry. However, previous studies have shown a fairly uniform progression of amyloid-β aggregation in APP/PS1 mice (Peng et al., 2016). We have also not measured changes in cerebral blood flow and volume which both have been shown to change during sleep (Klingelhöfer 2012; Turner et al., 2020; Bojarskaite et al., 2023). In our model, several different effects including vasodilation and vascular tone can potentially be quantified (Parker 2017), however the specific values of these changes remain for further study. The focus of this study was primarily to use elastography to establish some general trends in mice brains that can be replicated, validated, and correlated with other simultaneous measurements in future work, which could ideally also address the first two limitations. Despite these limitations, significant differences have been found with brain state, aging, and disease.

Overall, this study provides key new observations specifying cortical brain stiffness in wake and anesthetized states, in aging, and in disease mouse models of AQP4 deficiency and AD-related pathology using a high-resolution optical elastography method. Similarities between AQP4 deficiency and AD-related pathology in mice points to common glymphatic dysfunction between distinct conditions. This work is relevant to those interested in the biomechanical and biophysical properties of the brain's glymphatic system, as well as those interested in translating the methodology and analytical techniques to other imaging modalities for both mice and human studies.

Use of AI

No use of generative AI and AI-assisted technologies were used in the writing process.

Data and materials availability

All results data are available in the supplementary materials. Raw data and elastography code are available from the corresponding author on request, upon completion of a formal sharing agreement.

Funding

Funding was provided by Lundbeck Foundation grant R386-2021-165, Novo Nordisk Foundation grant NNF20OC0066419, National Institutes of Health grant R01AT011439, National Institutes of Health grant R21AG070331, National Institutes of Health grant U19NS128613, US Army Research Office grant MURI W911NF1910280, Human Frontier Science Program grant RGP0036, the Dr. Miriam and Sheldon G. Adelson Medical Research Foundation, and Simons Foundation grant 811237. Gary Ge is supported by the National Institute on Aging of the National Institutes of Health under award number F30AG069293. The content is solely the responsibility of the authors and does not necessarily represent the official views of the National Institutes of Health.

CRediT authorship contribution statement

Gary R. Ge: Writing – review & editing, Writing – original draft, Visualization, Software, Methodology, Investigation, Funding acquisition, Formal analysis, Conceptualization, Data curation, Project administration, Validation. **Wei Song:** Writing – review & editing, Methodology, Investigation, Validation. **Michael J. Giannetto:** Writing – review & editing, Methodology. **Jannick P. Rolland:** Writing – review & editing, Resources, Methodology, Formal analysis, Conceptualization, Funding acquisition, Project administration. **Maiken Nedergaard:** Writing – review & editing, Visualization, Resources, Methodology, Funding acquisition, Formal analysis, Conceptualization, Project administration, Supervision. **Kevin J. Parker:** Writing – review & editing, Writing – original draft, Visualization, Resources, Methodology, Funding acquisition, Formal analysis, Conceptualization, Project administration, Supervision.

Declaration of competing interest

Authors declare that they have no competing interests.

Data availability

All results data are available in the supplementary materials. Raw data and elastography code are available from the corresponding author on request, upon completion of a formal sharing agreement.

Acknowledgments

We acknowledge Dan Xue for their expert assistance in generating Fig. 5 as well as Benjamin Moon for generating Supplemental Fig. S1. We also thank Linda Weidman for proofreading the manuscript.

Supplementary materials

Supplementary material associated with this article can be found, in the online version, at doi:10.1016/j.neuroimage.2024.120662.

References

Arani, A., Murphy, M.C., Glaser, K.J., Manduca, A., Lake, D.S., Kruse, S.A., Jack, C.R., Ehman, R.L., Huston, J., 2015. Measuring the effects of aging and sex on regional brain stiffness with MR elastography in healthy older adults. Neuroimage 111, 59–64.

Beason-Held, L.L., Goh, J.O., An, Y., Kraut, M.A., Brien, R.J., Ferrucci, L., Resnick, S.M., 2013. Changes in brain function occur years before the onset of cognitive impairment. J. Neurosci. 33 (46), 18008.

Benveniste, H., Liu, X., Koundal, S., Sanggaard, S., Lee, H., Wardlaw, J., 2019. The glymphatic system and waste clearance with brain aging: a review. Gerontology 65 (2), 106–119.

Bigot, M., Chauveau, F., Beuf, O., Lambert, S.A., 2018. Magnetic resonance elastography of rodent brain. Front. Neurol. 9 (1010).

Bohr, T., Hjorth, P.G., Holst, S.C., Hrabětová, S., Kiviniemi, V., Lilius, T., Lundgaard, I., Mardal, K.A., Martens, E.A., Mori, Y., Nägerl, U.V., Nicholson, C., Tannenbaum, A.,

Thomas, J.H., Tithof, J., Benveniste, H., Iliff, J.J., Kelley, D.H., Nedergaard, M., 2022. The glymphatic system: current understanding and modeling. iScience 25 (9).
Bojarskaite, L., Vallet, A., Bjørnstad, D.M., Gullestad Binder, K.M., Cunen, C., Heuser, K., Kuchta, M., Mardal, K.A., Enger, R., 2023. Sleep cycle-dependent vascular dynamics in male mice and the predicted effects on perivascular cerebrospinal fluid flow and solute transport. Nat. Commun. 14 (1), 953.
Clayton, E.H., Garbow, J.R., Bayly, P.V., 2011. Frequency-dependent viscoelastic parameters of mouse brain tissue estimated by MR elastography. Phys. Med. Biol. 56 (8), 2391–2406.
Clayton, E.H., Genin, G.M., Bayly, P.V., 2012. Transmission, attenuation and reflection of shear waves in the human brain. J. R. Soc. Interface 9 (76), 2899–2910.
Coelho, A., Sousa, N., 2022. Magnetic resonance elastography of the ageing brain in normal and demented populations: A systematic review. Hum. Brain Mapp. 43 (13), 4207–4218.
Doyley, M.M., Parker, K.J., 2014. Elastography: general principles and clinical applications. Ultrasound. Clin. 9 (1), 1–11.
ElSheikh, M., Arani, A., Perry, A., Boeve, B.F., Meyer, F.B., Savica, R., Ehman, R.L., Huston, J., 2017. MR elastography demonstrates unique regional brain stiffness patterns in dementias. Am. J. Roentgenol. 209 (2), 403–408.
Ertl, M., Raasch, N., Hammel, G., Harter, K., Lang, C., 2018. Transtemporal investigation of brain parenchyma elasticity using 2-D shear wave elastography: definition of age-matched normal values. Ultrasound Med. Biol. 44 (1), 78–84.
Jr Ford, M.R., W, J.D., Rollins, A.M., Roy, A.S., Hu, Z., 2011. Method for optical coherence elastography of the cornea. J. Biomed. Opt. 16 (1), 1–7, 7.
Fujimoto, J.G., Pitris, C., Boppart, S.A., Brezinski, M.E., 2000. Optical coherence tomography: an emerging technology for biomedical imaging and optical biopsy. Neoplasia 2 (1), 9–25.
Ge, G.R., Rolland, J.P., Song, W., Nedergaard, M., Parker, K.J., 2023. Fluid compartments influence elastography of the aging mouse brain. Phys. Med. Biol. 68 (9), 095004.
Ge, G.R., Song, W., Nedergaard, M., Rolland, J.P., Parker, K.J., 2022. Theory of sleep/wake cycles affecting brain elastography. Phys. Med. Biol. 67 (22), 225013.
Gerischer, L.M., Fehlner, A., Köbe, T., Prehn, K., Antonenko, D., Grittner, U., Braun, J., Sack, I., Flöel, A., 2018. Combining viscoelasticity, diffusivity and volume of the hippocampus for the diagnosis of Alzheimer's disease based on magnetic resonance imaging. NeuroImage Clinical 18, 485–493.
Giannetto, M., Xia, M., Stæger, F.F., Metcalfe, T., Vinitsky, H.S., Dang, J.A.M.L., Xavier, A.L.R., Kress, B.T., Nedergaard, M., Hablitz, L.M., 2020. Biological sex does not predict glymphatic influx in healthy young, middle aged or old mice. Sci. Rep. 10 (1), 16073.
Gottschalk, A., Scafidi, S., Toung, T.J.K., 2021. Brain water as a function of age and weight in normal rats. PLoS One 16 (9), e0249384.
Guo, J., Bertalan, G., Meierhofer, D., Klein, C., Schreyer, S., Steiner, B., Wang, S., Vieira da Silva, R., Infante-Duarte, C., Koch, S., Boehm-Sturm, P., Braun, J., Sack, I., 2019. Brain maturation is associated with increasing tissue stiffness and decreasing tissue fluidity. Acta Biomater.
Hablitz, L.M., Nedergaard, M., 2021. The glymphatic system: a novel component of fundamental neurobiology. J. Neurosci. 41 (37), 7698.
Hablitz, L.M., Plá, V., Giannetto, M., Vinitsky, H.S., Stæger, F.F., Metcalfe, T., Nguyen, R., Benrais, A., Nedergaard, M., 2020. Circadian control of brain glymphatic and lymphatic fluid flow. Nat. Commun. 11 (1), 4411.
Hablitz, L.M., Vinitsky, H.S., Sun, Q., Stæger, F.F., Sigurdsson, B., Mortensen, K.N., Lilius, T.O., Nedergaard, M., 2019. Increased glymphatic influx is correlated with high EEG delta power and low heart rate in mice under anesthesia. Sci. Adv. 5 (2), eaav5447.
Hiscox, L.V., Johnson, C.L., Barnhill, E., McGarry, M.D.J., Huston, J., van Beek, E.J.R., Starr, J.M., Roberts, N., 2016. Magnetic resonance elastography (MRE) of the human brain: technique, findings and clinical applications. Phys. Med. Biol. 61 (24), R401–R437.
Hiscox, L.V., Johnson, C.L., McGarry, M.D.J., Perrins, M., Littlejohn, A., van Beek, E.J.R., Roberts, N., Starr, J.M., 2018. High-resolution magnetic resonance elastography reveals differences in subcortical gray matter viscoelasticity between young and healthy older adults. Neurobiol. Aging 65, 158–167.
Hiscox, L.V., Schwarb, H., McGarry, M.D.J., Johnson, C.L., 2021. Aging brain mechanics: Progress and promise of magnetic resonance elastography. Neuroimage 232, 117889.
Huang, D., Swanson, E.A., Lin, C.P., Schuman, J.S., Stinson, W.G., Chang, W., Hee, M.R., Flotte, T., Gregory, K., Puliafito, C.A., 1991. Optical coherence tomography. Science 254 (5035), 1178 (1979).
Jessen, N.A., Munk, A.S.F., Lundgaard, I., Nedergaard, M., 2015. The glymphatic system: a Beginner's guide. Neurochem. Res. 40 (12), 2583–2599.
Kedarasetti, R.T., Drew, P.J., Costanzo, F., 2022. Arterial vasodilation drives convective fluid flow in the brain: a poroelastic model. Fluids Barriers CNS 19 (1), 34.
Kennedy, B.F., Hillman, T.R., McLaughlin, R.A., Quirk, B.C., Sampson, D.D., 2009. *In vivo* dynamic optical coherence elastography using a ring actuator. Opt. Express 17 (24), 21762–21772.
Kennedy, B.F., Liang, X., Adie, S.G., Gerstmann, D.K., Quirk, B.C., Boppart, S.A., Sampson, D.D., 2011. *In vivo* three-dimensional optical coherence elastography. Opt. Express 19 (7), 6623–6634.
Kennedy, K.M., McLaughlin, R.A., Kennedy, B.F., Tien, A., Latham, B., Saunders, C.M., Sampson, D.D., 2013. Needle optical coherence elastography for the measurement of microscale mechanical contrast deep within human breast tissues. J. Biomed. Opt. 18 (12), 1–9, 9.
Klingelhöfer, J., 2012. Cerebral blood flow velocity in sleep. Perspect. Med. 1 (1), 275–284.
Kress, B.T., Iliff, J.J., Xia, M., Wang, M., Wei, H.S., Zeppenfeld, D., Xie, L., Kang, H., Xu, Q., Liew, J.A., Plog, B.A., Ding, F., Deane, R., Nedergaard, M., 2014. Impairment of paravascular clearance pathways in the aging brain. Ann. Neurol. 76 (6), 845–861.
Leartprapun, N., Adie, S.G., 2023. Recent advances in optical elastography and emerging opportunities in the basic sciences and translational medicine [Invited]. Biomed. Opt. Express 14 (1), 208–248.
Lerch, J.P., Carroll, J.B., Dorr, A., Spring, S., Evans, A.C., Hayden, M.R., Sled, J.G., Henkelman, R.M., 2008. Cortical thickness measured from MRI in the YAC128 mouse model of Huntington's disease. Neuroimage 41 (2), 243–251.
Loupas, T., Peterson, R.B., Gill, R.W., 1995. Experimental evaluation of velocity and power estimation for ultrasound blood flow imaging, by means of a two-dimensional autocorrelation approach. IEEe Trans. Ultrason. Ferroelectr. Freq. Control 42 (4), 689–699.
Low, G., Kruse, S.A., Lomas, D.J., 2016. General review of magnetic resonance elastography. World J. Radiol. 8 (1), 59–72.
Ma, Q., Ineichen, B.V., Detmar, M., Proulx, S.T., 2017. Outflow of cerebrospinal fluid is predominantly through lymphatic vessels and is reduced in aged mice. Nat. Commun. 8 (1), 1434.
Mestre, H., Hablitz, L.M., Xavier, A.L.R., Feng, W., Zou, W., Pu, T., Monai, H., Murlidharan, G., Castellanos Rivera, R.M., Simon, M.J., Pike, M.M., Plá, V., Du, T., Kress, B.T., Wang, X., Plog, B.A., Thrane, A.S., Lundgaard, I., Abe, Y., Yasui, M., Thomas, J.H., Xiao, M., Hirase, H., Asokan, A., Iliff, J.J., Nedergaard, M., 2018. Aquaporin-4-dependent glymphatic solute transport in the rodent brain. Elife 7, e40070.
Mestre, H., Mori, Y., Nedergaard, M., 2020. The brain's glymphatic system: current controversies. Trends Neurosci. 43 (7), 458–466.
Mestre, H., Verma, N., Greene, T.D., Lin, L.A., Ladron-de-Guevara, A., Sweeney, A.M., Liu, G., Thomas, V.K., Galloway, C.A., de Mesy Bentley, K.L., Nedergaard, M., Mehta, R.I., 2022. Periarteriolar spaces modulate cerebrospinal fluid transport into brain and demonstrate altered morphology in aging and Alzheimer's disease. Nat. Commun. 13 (1), 3897.
Mitchell, G.F., Parise, H., Benjamin, E.J., Larson, M.G., Keyes, M.J., Vita, J.A., Vasan, R. S., Levy, D., 2004. Changes in arterial stiffness and wave reflection with advancing age in healthy men and women. Hypertension 43 (6), 1239–1245.
Murali, S., Thompson, K.P., Rolland, J.P., 2009. Three-dimensional adaptive microscopy using embedded liquid lens. Opt. Lett. 34 (2), 145–147.
Murphy, M.C., Curran, G.L., Glaser, K.J., Rossman, P.J., Huston, J., Poduslo, J.F., Jack, C. R., Felmlee, J.P., Ehman, R.L., 2012. Magnetic resonance elastography of the brain in a mouse model of Alzheimer's disease: initial results. Magn. Reson. Imaging 30 (4), 535–539.
Murphy, M.C., Huston Iii, J., Jack Jr, C.R., Glaser, K.J., Manduca, A., Felmlee, J.P., Ehman, R.L., 2011. Decreased brain stiffness in Alzheimer's disease determined by magnetic resonance elastography. J. Magn. Reson. Imaging 34 (3), 494–498.
Murphy, M.C., Huston, J., Ehman, R.L., 2019. MR elastography of the brain and its application in neurological diseases. Neuroimage 187, 176–183.
Nedergaard, M., Goldman, S.A., 2020. Glymphatic failure as a final common pathway to dementia. Science 370 (6512), 50–56 (1979).
Ormachea, J., Castaneda, B., Parker, K.J., 2018. Shear wave speed estimation using reverberant shear wave fields: implementation and feasibility studies. Ultrasound Med. Biol. 44 (5), 963–977.
Ormachea, J., Parker, K.J., 2020. Elastography imaging: the 30 year perspective. Phys. Med. Biol. 65 (24), 24TR06.
Parker, K.J., 2017. Are rapid changes in brain elasticity possible? Phys. Med. Biol. 62 (18), 7425–7439.
Parker, K.J., Ormachea, J., Zvietcovich, F., Castaneda, B., 2017. Reverberant shear wave fields and estimation of tissue properties. Phys. Med. Biol. 62 (3), 1046–1061.
Peng, W., Achariyar, T.M., Li, B., Liao, Y., Mestre, H., Hitomi, E., Regan, S., Kasper, T., Peng, S., Ding, F., Benveniste, H., Nedergaard, M., Deane, R., 2016. Suppression of glymphatic fluid transport in a mouse model of Alzheimer's disease. Neurobiol. Dis. 93, 215–225.
Rasmussen, M.K., Mestre, H., Nedergaard, M., 2021. Fluid transport in the brain. Physiol. Rev. 102 (2), 1025–1151.
Reeves, B.C., Karimy, J.K., Kundishora, A.J., Mestre, H., Cerci, H.M., Matouk, C., Alper, S.L., Lundgaard, I., Nedergaard, M., Kahle, K.T., 2020. Glymphatic system impairment in Alzheimer's Disease and idiopathic normal pressure hydrocephalus. Trends Mol. Med. 26 (3), 285–295.
Rolland, J.P., Meemon, P., Murali, S., Thompson, K.P., Lee, K.s., 2010. Gabor-based fusion technique for optical coherence microscopy. Opt. Express 18 (4), 3632–3642.
Sack, I., 2023. Magnetic resonance elastography from fundamental soft-tissue mechanics to diagnostic imaging. Nat. Rev. Phys. 5 (1), 25–42.
Sack, I., Streitberger, K.J., Krefting, D., Paul, F., Braun, J., 2011. The influence of physiological aging and atrophy on brain viscoelastic properties in humans. PLoS One 6 (9), e23451.
Santelices, L.C., Rutman, S.J., Prantil-Baun, R., Vorp, D.A., Ahearn, J.M., 2008. Relative contributions of age and atherosclerosis to vascular stiffness. Clin. Transl. Sci. 1 (1), 62–66.
Segel, M., Neumann, B., Hill, M.F.E., Weber, I.P., Viscomi, C., Zhao, C., Young, A., Agley, C.C., Thompson, A.J., Gonzalez, G.A., Sharma, A., Holmqvist, S., Rowitch, D. H., Franze, K., Franklin, R.J.M., Chalut, K.J., 2019. Niche stiffness underlies the ageing of central nervous system progenitor cells. Nature 573 (7772), 130–134.
Silva, I., Silva, J., Ferreira, R., Trigo, D., 2021. Glymphatic system, AQP4, and their implications in Alzheimer's disease. Neurol. Res. Pract. 3 (1), 5.
Takamura, T., Motosugi, U., Sasaki, Y., Kakegawa, T., Sato, K., Glaser, K.J., Ehman, R.L., Onishi, H., 2019. Influence of age on global and regional brain stiffness in young and middle-aged adults. J. Magn. Reson. Imaging 51 (3), 727–733.

Thomas, J.H., 2022. Theoretical analysis of wake/sleep changes in brain solute transport suggests a flow of interstitial fluid. Fluids Barriers CNS 19 (1), 30.
Thrane, A.S., Rappold, P.M., Fujita, T., Torres, A., Bekar, L.K., Takano, T., Peng, W., Wang, F., Rangroo Thrane, V., Enger, R., Haj-Yasein, N.N., Skare, Ø., Holen, T., Klungland, A., Ottersen, O.P., Nedergaard, M., Nagelhus, E.A., 2011. Critical role of aquaporin-4 (AQP4) in astrocytic Ca2+ signaling events elicited by cerebral edema. Proc. Natl. Acad. Sci. 108 (2), 846–851.
Tithof, J., Boster, K.A.S., Bork, P.A.R., Nedergaard, M., Thomas, J.H., Kelley, D.H., 2022. A network model of glymphatic flow under different experimentally-motivated parametric scenarios. iScience 25 (5).
Turner, K.L., Gheres, K.W., Proctor, E.A., Drew, P.J., 2020. Neurovascular coupling and bilateral connectivity during NREM and REM sleep. Elife 9, e62071.
Tzschätzsch, H., Kreft, B., Schrank, F., Bergs, J., Braun, J., Sack, I., 2018. *In vivo* time-harmonic ultrasound elastography of the human brain detects acute cerebral stiffness changes induced by intracranial pressure variations. Sci. Rep. 8 (1), 17888.
van der Flier, W.M., de Vugt, M.E., Smets, E.M.A., Blom, M., Teunissen, C.E., 2023. Towards a future where Alzheimer's disease pathology is stopped before the onset of dementia. Nat. Aging 3 (5), 494–505.
Wang, J., Tanila, H., Puoliväli, J., Kadish, I., v. Groen, T., 2003. Gender differences in the amount and deposition of amyloidβ in APPswe and PS1 double transgenic mice. Neurobiol. Dis. 14 (3), 318–327.
Wang, S., Larin, K.V., 2015. Optical coherence elastography for tissue characterization: a review. J. Biophotonics 8 (4), 279–302.
Xie, L., Kang, H., Xu, Q., Chen, M.J., Liao, Y., Thiyagarajan, M., O'Donnell, J., Christensen, D.J., Nicholson, C., Iliff, J.J., Takano, T., Deane, R., Nedergaard, M., 2013. Sleep drives metabolite clearance from the adult brain. Science 342 (6156), 373–377 (1979).
Xu, D., Wen, Z., Coleto, A.G., Pomerantz, M., Lambropoulos, J.C., Rolland, J.P., 2021. Verification of cascade optical coherence tomography for freeform optics form metrology. Opt. Express 29 (6), 8542–8552.
Xu, Z., Xiao, N., Chen, Y., Huang, H., Marshall, C., Gao, J., Cai, Z., Wu, T., Hu, G., Xiao, M., 2015. Deletion of aquaporin-4 in APP/PS1 mice exacerbates brain Aβ accumulation and memory deficits. Mol. Neurodegener. 10 (1), 58.
Zvietcovich, F., Larin, K.V., 2022. Wave-based optical coherence elastography: the 10-year perspective. Prog. Biomed. Eng. 4 (1), 012007.
Zvietcovich, F., Pongchalee, P., Meemon, P., Rolland, J.P., Parker, K.J., 2019. Reverberant 3D optical coherence elastography maps the elasticity of individual corneal layers. Nat. Commun. 10 (1), 4895.
Zysk, A.M., Nguyen, F.T., Oldenburg, A.L., Marks, D.L., 2007. Optical coherence tomography: a review of clinical development from bench to bedside. J. Biomed. Opt. 12 (5), 1–21, 21.